NeuroImage 188 (2019) 357–368

Contents lists available at ScienceDirect

NeuroImage

journal homepage: www.elsevier.com/locate/neuroimage

Changes in functional connectivity dynamics with aging: A dynamical phase synchronization approach

Sou Nobukawa [a], Mitsuru Kikuchi [b], Tetsuya Takahashi [b,c,*]

[a] Department of Computer Science, Chiba Institute of Technology, 2-17-1 Tsudanuma, Narashino, Chiba, 275–0016, Japan
[b] Research Center for Child Mental Development, Kanazawa University, 13–1 Takaramachi, Kanazawa, Ishikawa, 920–8640, Japan
[c] Department of Neuropsychiatry, University of Fukui, 23–3 Matsuokashimoaizuki, Eiheiji, Yoshida, Fukui, 910–1193, Japan

ARTICLE INFO

Keywords:
Dynamical network
Aging
Functional connectivity
Electroencephalogram
Instantaneous phase synchronization
Multiscale entropy
Phase lag index

ABSTRACT

The dynamics of the human brain network has attracted broad attention, in recognition of the concept that functional connectivity is not static, but changes its pattern over time, even in the resting state. We hypothesized that analysis of continuously captured time-varying instantaneous phase synchronization between signals from different brain regions might add another dimension to already identified network dynamics. To validate this hypothesis as an aid to elucidating the physiological mechanisms of aging, we examined time-series of instantaneous phase synchronization events in resting-state EEG activity across the brain, in healthy younger and healthy older subjects. We then characterized the temporal dynamics of phase synchronization using multiscale entropy, which quantifies the complexity of brain signal dynamics over multiple time scales. The results of surrogate analyses confirmed that the temporal dynamics of phase synchronization arise from deterministic processes in the neural network system. Group comparison showed region-specific enhanced complexity of temporal dynamics of phase synchronization in older subjects in alpha band predominantly in frontal brain regions, which was not identified by a comparative phase synchronization approach such as phase lag index. Enhanced complexity of temporal dynamics of functional connectivity in older subjects might reflect a general network alteration theory in aging. This is a first report describing the importance of capturing the dynamics of instantaneous phase synchronization and characterizing its temporal organization. Applying this method to neurophysiologic data may provide a novel understanding of dynamical neural network processes in both healthy and pathological conditions.

1. Introduction

Recent findings in network studies of the human brain support the concept that brain function emerges from the topological features of the whole brain network, not merely from the separate actions of individual regions (van den Heuvel and Sporns, 2013; Sporns, 2014; Bassett and Sporns, 2017). Over the past decade, an ambitious effort has been made to describe the human brain connectivity network, known as the human "connectome" (Glasser et al., 2016a, 2016b). Meanwhile, increasing studies using both structural and functional approaches have been applied fruitfully for the assessment of both healthy and pathological conditions, along with recent progress in neuroimaging techniques and analytic methods (Aertsen et al., 1989; Friston et al., 1993; Hagmann et al., 2007; Schmahmann et al., 2007). At the structural level, the development of diffusion tensor imaging (DTI) enabled detailed in vivo characterization of white matter projections, and has elucidated developmental (Barnea-Goraly et al., 2005; Asato et al., 2010; Blakemore et al., 2010), aging-related (Pfefferbaum et al., 2000; Nusbaum et al., 2001; O'Sullivan et al., 2001; Grieve et al., 2007; Madden et al., 2007; Bucur et al., 2008; Sullivan et al., 2010), and pathological (e.g., schizophrenia (Kubicki et al., 2005; Samartzis et al., 2014), Alzheimer's disease (Stebbins and Murphy, 2009; Zhang et al., 2007)) processes.

The functional connectivity approach has its roots in the fact that the brain network integrates information and plays a crucial role in optimal brain function (Buzsáki and Draguhn, 2004; Fries, 2005; Varela et al., 2001; Hutchison et al., 2013; Koutsoukos et al., 2015). Functional MRI is a widely used neuroimaging modality for exploring functional connectivity, with a high spatial resolution. However, blood oxygenation level-dependent signals are an indirect measure of neuronal activity and have limited temporal resolution (Logothetis, 2008). In contrast, despite

* Corresponding author. Research Center for Child Mental Development, Kanazawa University, 13–1 Takaramachi, Kanazawa, Ishikawa, 920–8640, Japan.
E-mail address: takahash@u-fukui.ac.jp (T. Takahashi).

https://doi.org/10.1016/j.neuroimage.2018.12.008
Received 2 June 2018; Received in revised form 15 October 2018; Accepted 4 December 2018
Available online 7 December 2018
1053-8119/

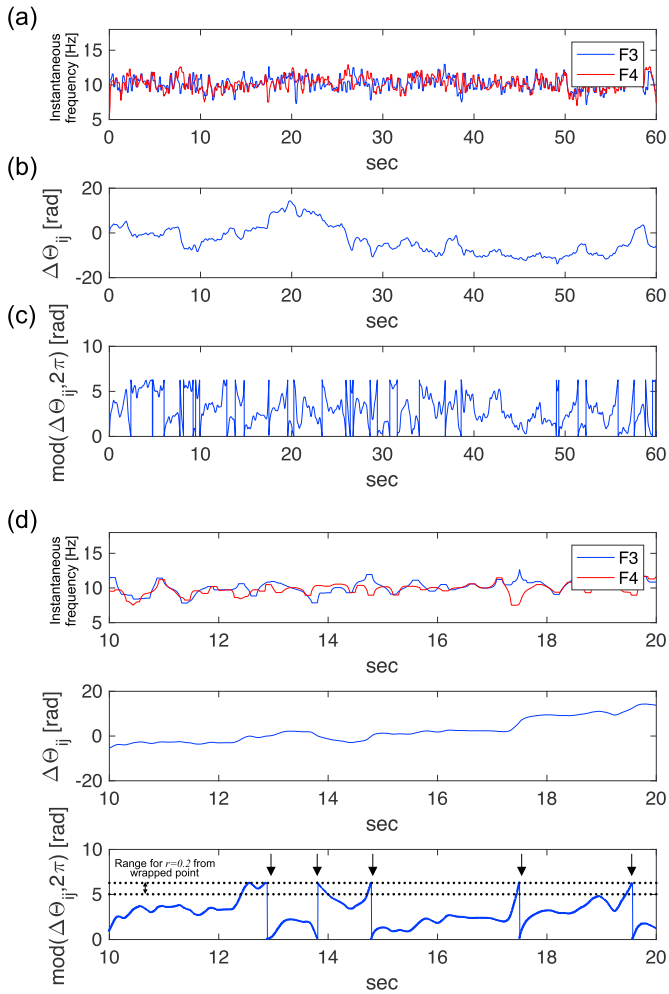

Fig. 1. (a) Typical example of a time-series of instantaneous frequency for a younger subject. (b) Time-series of unwrapped phase differences $\Delta\Theta_{i,j}(t)$ (i: F3 node, j: F4 node) for the same younger subject. (c) Wrapped phase differences $\mathrm{mod}(\Delta\Theta_{i,j}(t), 2\pi)$ of the time-series as shown in (b). (d) Expanded portions of (a), (b) and (c). Here, the arrows indicate wrapping points.

its low spatial resolution, the electroencephalogram (EEG) records the electrical fields generated by the cortex directly, with excellent temporal resolution. Traditionally, the functional connectivity reflected in EEG has been quantified by coherence, correlation and mutual information, i.e., synchronization of neural activity between brain regions (Aertsen et al., 1989; Friston et al., 1993; Bullmore and Sporns, 2009). A recent evaluation of phase synchrony tackled the problem of volume conduction and was able to achieve fine temporal resolution for functional connectivity (Nunez et al., 1997; Nolte et al., 2004) using measures such as synchronization likelihood (Stam and Van Dijk, 2002) and phase lag index (PLI) (Stam et al., 2007). This demonstration of the value of phase dynamics has opened a new avenue for the evaluation of brain networks. For example, the phase synchrony approach has demonstrated that the brain network has feedback loops at multiple hierarchical levels, with complex network characteristics (Eguiluz et al., 2005; van den Heuvel et al., 2008; van den Heuvel and Sporns, 2013; Pendl et al., 2017). It has also identified the networks implementing perception and cognitive functions (Bullmore and Sporns, 2009), and has elucidated the characteristics of these networks in both healthy (Bullmore and Sporns, 2009) and pathological (Stam et al., 2006; Stam et al., 2009; Bassett et al., 2009; Bullmore and Sporns, 2009; Engels et al., 2015; Takahashi et al., 2017; Takahashia et al.) conditions (reviewed in (Uhlhaas and Singer, 2006; Stam, 2014; Voytek and Knight, 2015)).

The spatiotemporal dynamics of brain networks have recently attracted broad attention, in recognition of the concept that functional connectivity is not static (Allen et al., 2014; Betzel et al. Sporns; Calhoun et al., 2014). Brain networks change dynamically in response to different contexts or varying external stimuli, even in the resting state (Allen et al., 2014; Betzel et al. Sporns; Calhoun et al., 2014; Zalesky et al., 2014; Betzel et al., 2016). Moreover, brain network dynamics have been shown to associate with learning (Bassett et al., 2011; Telesford et al. Bassett), cognitive function (Braun et al., 2015; Davison et al., 2015), healthy aging (Chen et al., 2018; Tian et al., 2018), and some psychiatric disorders (Zhang et al., 2016). However, previous studies have examined network dynamics by calculating variation in averaged functional connectivity using predefined time windows (Allen et al., 2014; Betzel et al. Sporns; Calhoun et al., 2014; Zalesky et al., 2014; Bassett et al., 2011; Telesford et al. Bassett; Braun et al., 2015; Davison et al., 2015; Zhang et al., 2016; Chen et al., 2017; Chen et al., 2018), an approach that ignores moment-to-moment dynamics across multiple time-scales, from milliseconds to minutes (Garrett et al., 2013). Despite the importance of examining time-varying functional connectivity for clarifying how widely separated areas of the brain communicate with one another, far fewer studies have addressed this issue (Tass et al., 1998). We hypothesized that analyzing time-variations in instantaneous phase synchronization between signals from different brain regions could add another dimension to the understanding of network dynamics. This study aimed to validate our hypothesis, in the context of elucidating the physiological mechanisms of aging. We examined time-varying instantaneous phase synchronization (referred to as dynamical phase synchronization: DPS) of resting-state EEG activity across the brain in healthy younger and healthy older subjects. We then characterized its dynamical pattern using multiscale entropy (MSE) analysis, which quantifies the variability of a signal at multiple time-scales (Garrett et al., 2013).

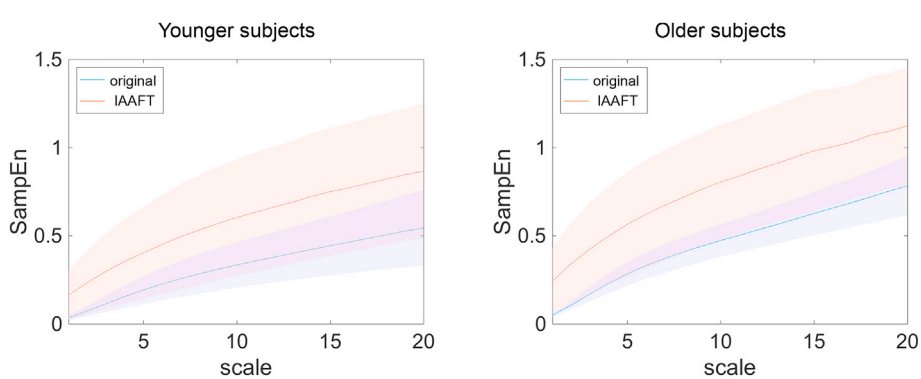

Fig. 2. Sample entropy (SampEn) of time-series of wrapped phase differences $\mathrm{mod}(\Delta\Theta_{i,j}(t), 2\pi)$ (i: F3 node, j: F4 node) (original) and the corresponding iterated amplitude-adjusted Fourier-transformed (IAAFT) data in the younger group (left) and older group (right). The lines and shaded area indicate the mean and standard deviation in each time-series.

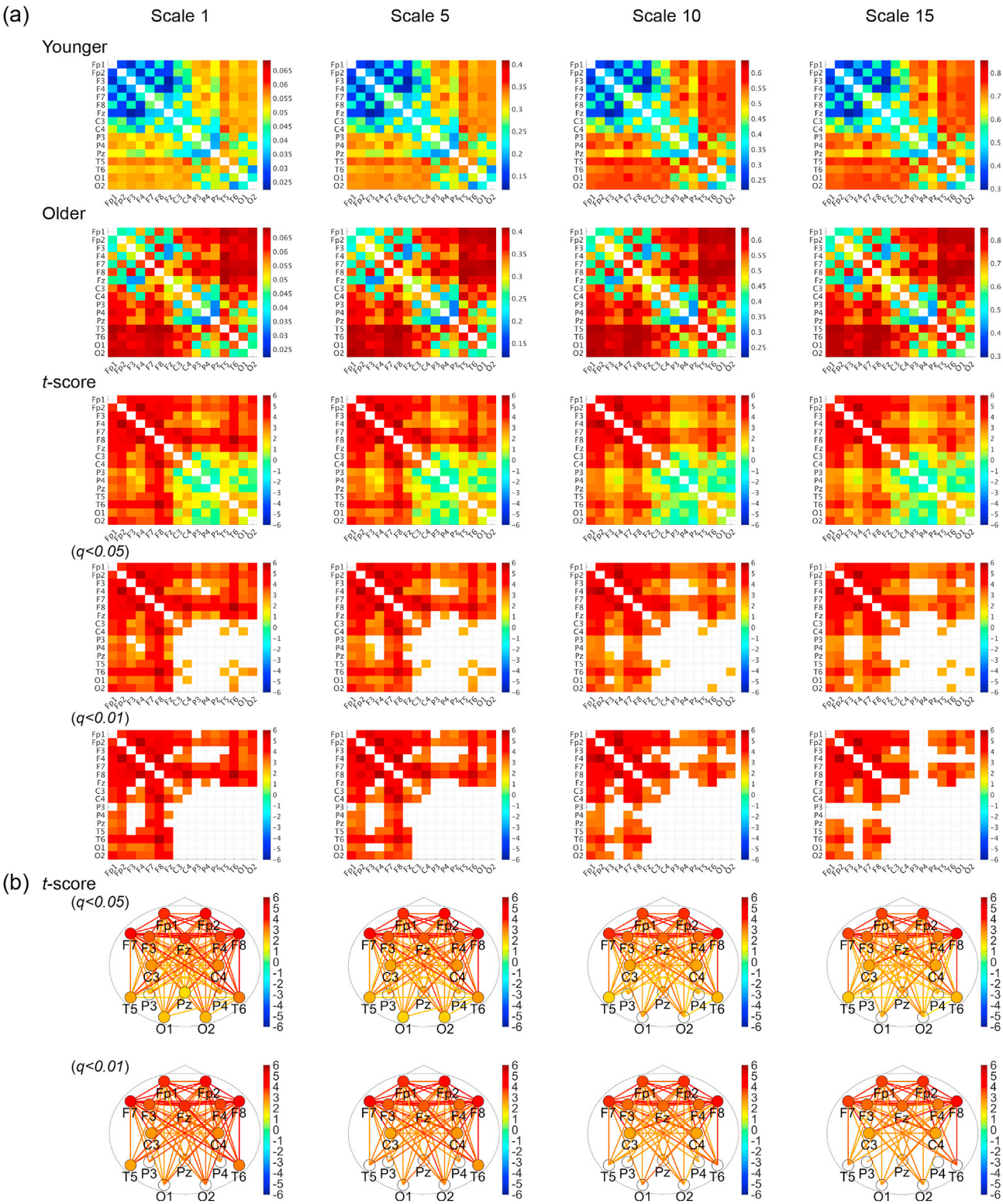

Fig. 3. (a) Mean values of sample entropy (SampEn) in the younger group (upper part) and the older group (middle part). *t*-scores for differences between the younger and older groups, adjusted for false discovery rate (FDR) $q < 0.05, 0.01$ (bottom part). (b) *t*-scores adjusted for FDR: $q < 0.05, 0.01$ and *t*-scores for node degree of SampEn across the topography.

2. Materials and methods

2.1. Participants

This study was performed at the Department of Neuropsychiatry, Kanazawa University, Japan. In this study, 29 healthy younger subjects (14 male, 15 female; average age, 22.9 years; standard deviation (SD), 2.7 years; age range, 20 – 28 years) participated along with 18 healthy older subjects (7 male, 11 female; average age, 57.5 years; SD, 4.7 years; age range, 51 – 67 years). These groups were sex-matched ($\chi^2 = 0.39$,

Table 1
ANOVA results for the node degree of sample entropy (SampEn) for mod($\Delta\Theta_{i,j}$, 2π). For clarity, values with $p < 0.05$ are shown in bold.

Group × scale × electrode	$\mathbf{F} = 12.4, \mathbf{p} = 3.0 \times 10^{-8}, \boldsymbol{\eta}^2 = 0.21$
Group × scale	$\mathbf{F} = 10.4, \mathbf{p} = 2.2 \times 10^{-3}, \boldsymbol{\eta}^2 = 0.18$
Group × electrode	$\mathbf{F} = 12.7, \mathbf{p} = 2.2 \times 10^{-8}, \boldsymbol{\eta}^2 = 0.22$
Group effect	$\mathbf{F} = 12.2, \mathbf{p} = 1.2 \times 10^{-3}, \boldsymbol{\eta}^2 = 0.21$

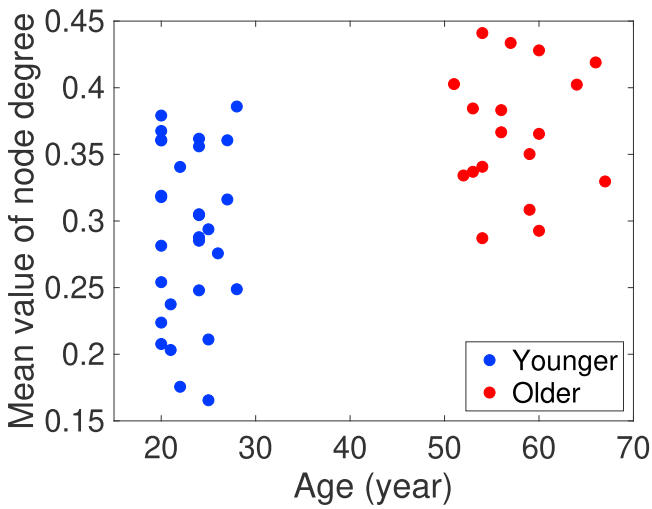

Fig. 4. Scatterplots for age and mean value of node degree among frontal electrodes (Fp1, Fp2, F3, F4, F7, F8 and Fz) for scale-1 sample entropy (SampEn) of dynamical phase synchronization (DPS).

$p = 0.52$). All subjects were nonsmokers and medication-free. Potential subjects with major medical or neurological conditions, including epilepsy, previous head trauma, or a lifetime history of alcohol or drug dependence, were excluded. The subjects with major brain abnormalities including remarkable vascular changes identified on conventional MRI were excluded. Additionally, older subjects with a Mini-Mental State Examination score of less than 27 were excluded. After a complete explanation of the study, written informed consent was obtained from each subject.

All methods were performed in accordance with the Declaration of Helsinki, and the protocol of the study was approved by the Ethics Committee of Kanazawa University.

2.2. EEG recording

The subjects were studied while seated in an electrically shielded, soundproof, light-controlled recording room. Standard scalp electrodes were placed in accordance with the International 10–20 System. EEG was recorded with an 18-channel electroencephalography system (EEG-4518, Nihon-Koden, Tokyo, Japan) at 16 electrodes sites: Fp1, Fp2, F3, Fz, F4, F7, F8, C3, C4, P3, Pz, P4, T5, T6, O1 and O2, referenced to physically linked ear-lobe electrodes. Eye movements were monitored using bipolar electro-oculography (EOG). The EEG signals (200 Hz sampling frequency) were recorded with a time constant of 0.3 s, and a 1.5–60 Hz bandpass filter. EEG signals were recorded for 10 − 15 min for each subject with the eyes closed in the resting condition. The subjects were observed via a video monitoring system. The state of vigilance of the subject was monitored during recording using the EEG traces, so that only epochs of eyes-closed wakefulness (and not light sleep) were analyzed.

Artifacts such as muscle activity, blinks, and eye movement were visually identified, and one continuous, artifact-free, 60-sec (12000 data points) epoch was extracted for each subject. For each epoch, bandpass filtering for the alpha band (8–13 [Hz]) was performed (see section 2.3.1). The first and last 5-sec period (1000 data point) in each bandpass-filtered epoch were removed to avoid distortions produced by the bandpass filtering process.

2.3. Dynamical phase synchronization

2.3.1. Phase difference eliminating phase slips

EEG signals were transformed to phase $\theta(t)$ $(-\pi \le \theta \le \pi)$ and amplitude space using the Hilbert transform. The unwrapped phase signal $\theta(t)$ was then transformed into an instantaneous frequency [Hz] signal by temporal subtraction. This instantaneous frequency signal is affected by phase noise, which becomes worse in relatively low power time-series (Cohen, 2014). Fortunately, alpha band activity shows clear oscillations with a relatively narrow bandwidth compared to other frequency bands, which is optimal for estimating instantaneous frequency in a way that is robust to background noise (Sameni and Seraj, 2017). Furthermore, physiological aging has been studied mainly in terms of alpha band activity (Ishii et al., 2017). Therefore, we focused on the dynamics of the alpha band in this study. However even in the alpha band time-series, during a period of phase noise the instantaneous frequency can deviate significantly from the frequency range of the alpha band, in events that are known as phase slips (Cohen, 2014). To avoid phase slips, we eliminated them from the time-series using a median filter with a degree of 40 (Cohen, 2014). Finally, by temporal integration of the median-filtered instantaneous frequency, an unwrapped phase signal without phase slips $\Theta(t)$ $(-\infty < \Theta(t) < +\infty)$ was derived.

We then estimated the time series of phase differences across electrodes as:

$$\Delta\Theta_{i,j}(t) = \Theta_i(t) - \Theta_j(t), \tag{1}$$

where i,j indicate the 16 electrodes. When calculating the MSE (see section 2.3.2), the directional trend of phase differences critically affects the results for $C_m(r)$, especially when the range of the trend is much larger than the time scale of the phase difference that we focus on. Therefore, to eliminate the influence of such trends, the phase differences were wrapped into units of radians, as mod($\Delta\theta_{i,j}, 2\pi$).

Fig. 1 shows typical examples of the time-series of instantaneous frequency [Hz] (a), $\Delta\Theta_{i,j}(t)$ (i: F3 node, j: F4 node) (b), mod($\Delta\theta_{i,j}, 2\pi$) (c), and their magnified figures (d) in a young subject. The time series of phase differences exhibits a complex pattern composed of both synchronous and asynchronous phase periods (Fig.1 (d), top panel). We define this pattern of dynamical synchronous and asynchronous phase differences as DPS.

2.3.2. Multiscale entropy analysis of dynamical phase synchronization

To characterize the temporal organization of DPS, we used MSE, which evaluates the complexity of the time series across multiple time-scales (Costa et al., 2002). For a random variable $\{x_1, x_2, \cdots x_N\}$ whose range is normalized to 1, the sample entropy (SampEn) is defined by

$$h(r,m) = -\log\frac{C_{m+1}(r)}{C_m(r)}, \tag{2}$$

where $C_m(r)$ indicates the probability of satisfying the inequality $\left|\mathbf{x}_i^m - \mathbf{x}_j^m\right| < r$ $(i \ne j, i,j = 1, 2, \cdots)$. Here, $\mathbf{x}_i^m$ is an m-dimensional vector given by

$$\mathbf{x}_i^m = \{x_i, x_{i+1}, \cdots, x_{i+m-1}\}. \tag{3}$$

In MSE analysis, the original time series $\{x_1, x_2, \cdots, x_N\}$ is rescaled with the scale factor τ $(\tau = 1, 2, \cdots)$ into a more coarse-grained time series:

$$y_j^{(\tau)} = \frac{1}{\tau}\sum_{i=(j-1)\tau+1}^{j_\tau} x_i, \qquad (1 \le j \le N/\tau) \tag{4}$$

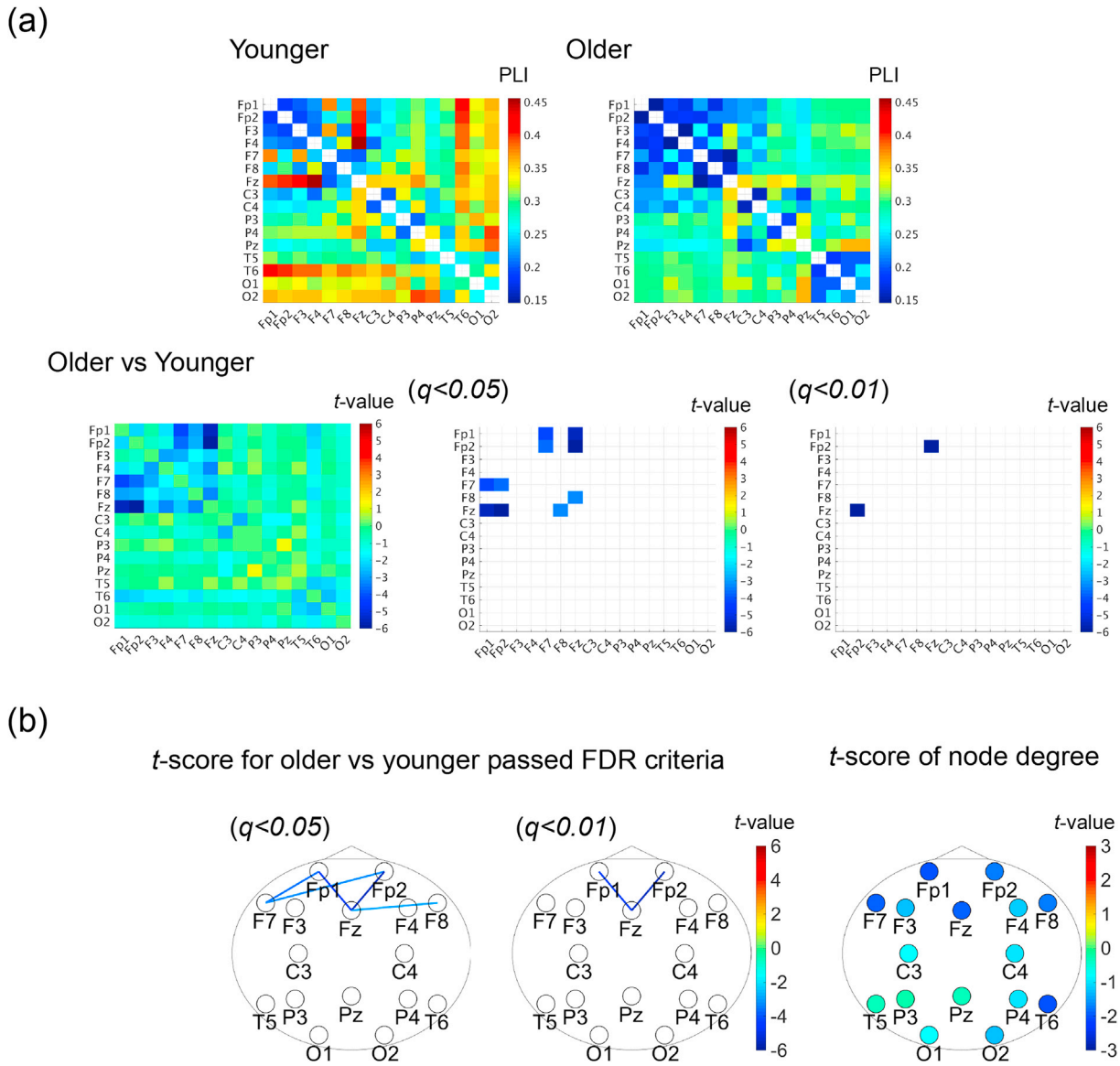

Fig. 5. (a) Mean values of phase lag index (PLI) in the younger group and older group (top parts). *t*-scores for differences between the younger and older groups adjusted for false discovery rate (FDR) $q < 0.05, q < 0.01$ (bottom parts). (b) *t*-scores adjusted for FDR: $q < 0.05$ (left),0.01 (middle) and *t*-scores for node degree across the topography. Here, no significant group differences in node degree were identified after adjustment for FDR: $q < 0.05$, 0.01. *t*-scores of node degree are represented by a narrow t range ($-3 \leq t \leq 3$) (right).

Table 2
ANOVA results for node degree of phase lag index (PLI). For clarity, values with $P < 0.05$ are shown in bold.

Group × electrode	$\mathbf{F} = 2.3, \mathbf{p} = 0.034, \boldsymbol{\eta}^2 = 4.9 \times 10^{-2}$
Group effect	$F = 1.3, p = 0.24, \eta^2 = 3.0 \times 10^{-2}$

The time-scaled sample entropy SampEn $h^{\tau}(r, m)$ is then calculated using the resulting coarse-grained series. We used the dependency of $h^{\tau}(r, m)$ on the scale factor τ to characterize the complexity of the time series of phase differences. In this study, we set $m = 2$ and $r = 0.2$ (Costa et al., 2002). In this analysis, phase discontinuities produced by the wrapping procedure for $\mathrm{mod}(\Delta\theta_{ij}, 2\pi)$, which can distort SampEn, can be eliminated by requiring $\left|\mathbf{x}_i^m - \mathbf{x}_j^m\right| < r$ for $C_m(r)$, because the size of the phase discontinuity ($\approx 2\pi$) is larger than the $r = 0.2$ range ($\approx 2\pi r = 0.62$) (see arrows in Fig. 1 (d)).

In addition, we calculated the node degrees of SampEn at each electrode, defined as the averages among links that connect to the remaining electrodes.

2.3.3. Surrogate analysis

To examine whether DPS reflects nonlinear deterministic processes, we derived a time-series of surrogate data for each subject using the iterated amplitude-adjusted Fourier transform (IAAFT) (Schreiber and Schmitz, 1996) against the original phase difference $\Delta\Theta_{ij}(t)$. In the surrogate process, the phase components of the signals are randomized. If the time-series is composed of nonlinear dynamics, MSE profiles of original time-series and their surrogates demonstrate a significant difference in both reduced and enhanced directions from the original directions (see "Appendix" section). This randomization should eliminate the nonlinear dynamics that result from the mutually correlated phase components of DPS generated in the neural network. In this study, the iteration time was set to 20 to reproduce the same power spectrum. We then compared the MSE profiles for the original data separated from each group and the corresponding surrogate data.

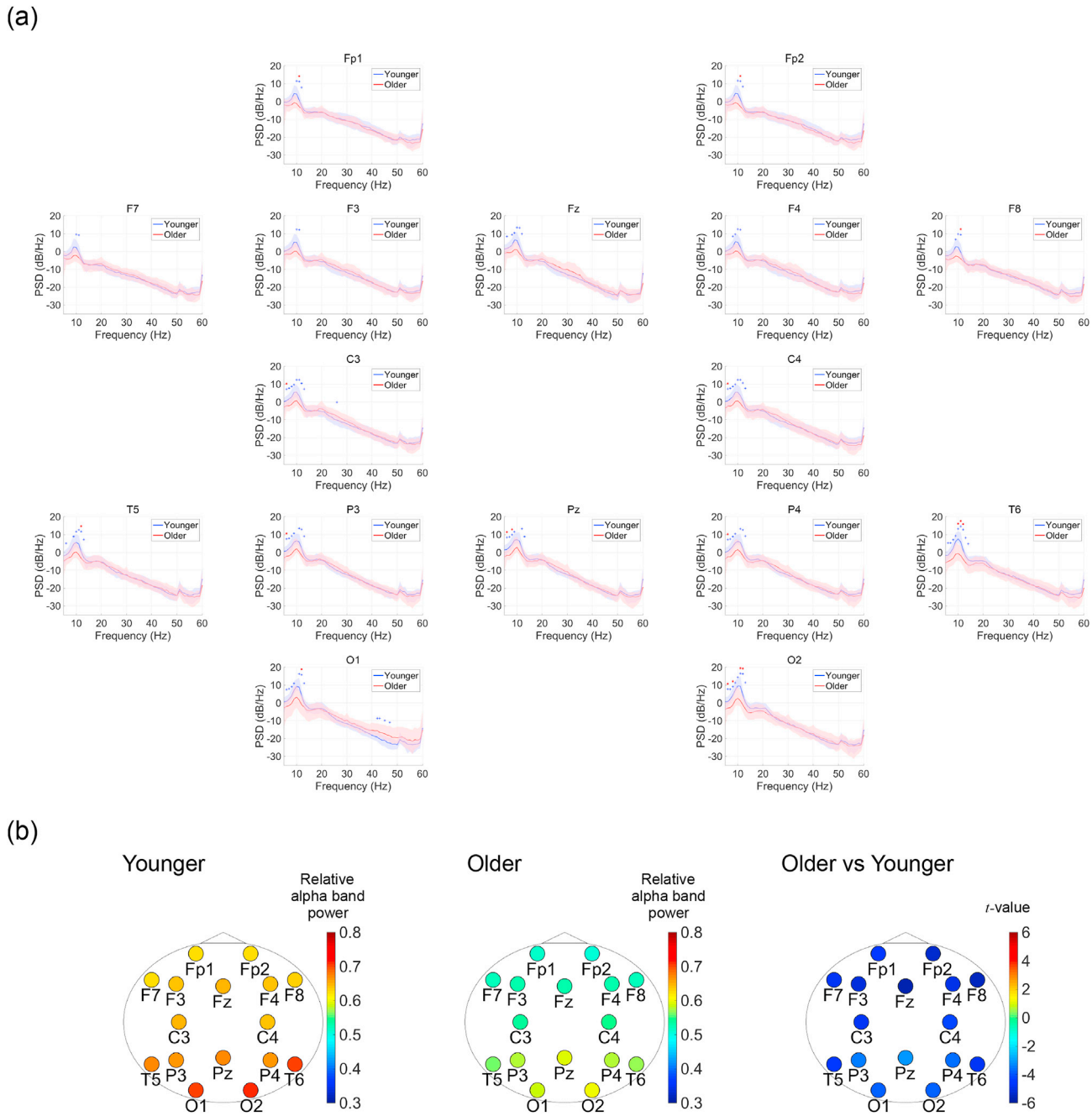

Fig. 6. (a) Power spectrum of EEG data for younger subjects and older subjects. The blue + and red * indicate differences that are significant after adjustment for false discovery rate (FDR) $q < 0.05, 0.01$, respectively. (b) Mean value of the relative power of alpha band and t-value between older vs younger groups. All electrodes passed FDR correction of $q < 0.01$.

Table 3
ANOVA results for the relative power of the alpha band. For clarity, values with $p < 0.05$ are shown in bold.

Group × electrode	$F = 1.47, p = 0.23, \eta^2 = 3.2 \times 10^{-2}$
Group effect	$\mathbf{F} = 41.1, \mathbf{p} = 7.6 \times 10^{-8}, \boldsymbol{\eta}^2 = 0.47$

2.4. Phase lag index

As a conventional method for estimating functional connectivity across electrodes, the phase lag index (PLI) has been widely utilized. The PLI determines functional connectivity by calculating the consistency in the distribution of instantaneous phase differences $\Delta\theta_{i,j}(t) = \theta_i(t) - \theta_j(t)$ (i, j indicate the 16 electrodes) defined as (Stam et al., 2007):

$$PLI_{ij} = \left| < \mathrm{sign}\left(\Delta\theta_{i,j}(t)\right) > \right|, \tag{5}$$

where $< \cdot >$ represents the time average. The PLI ranges between 0 (no phase coupling or a coupling phase difference of 0 modules π) and one (full phase coupling). In this study, the PLI was calculated for the same EEG data that were used for the DPS analysis, but the data were segmented into 5 s (1000 data points) epochs (a total of 10 epochs for each subject). In addition, we calculated the node degree of PLI at each node.

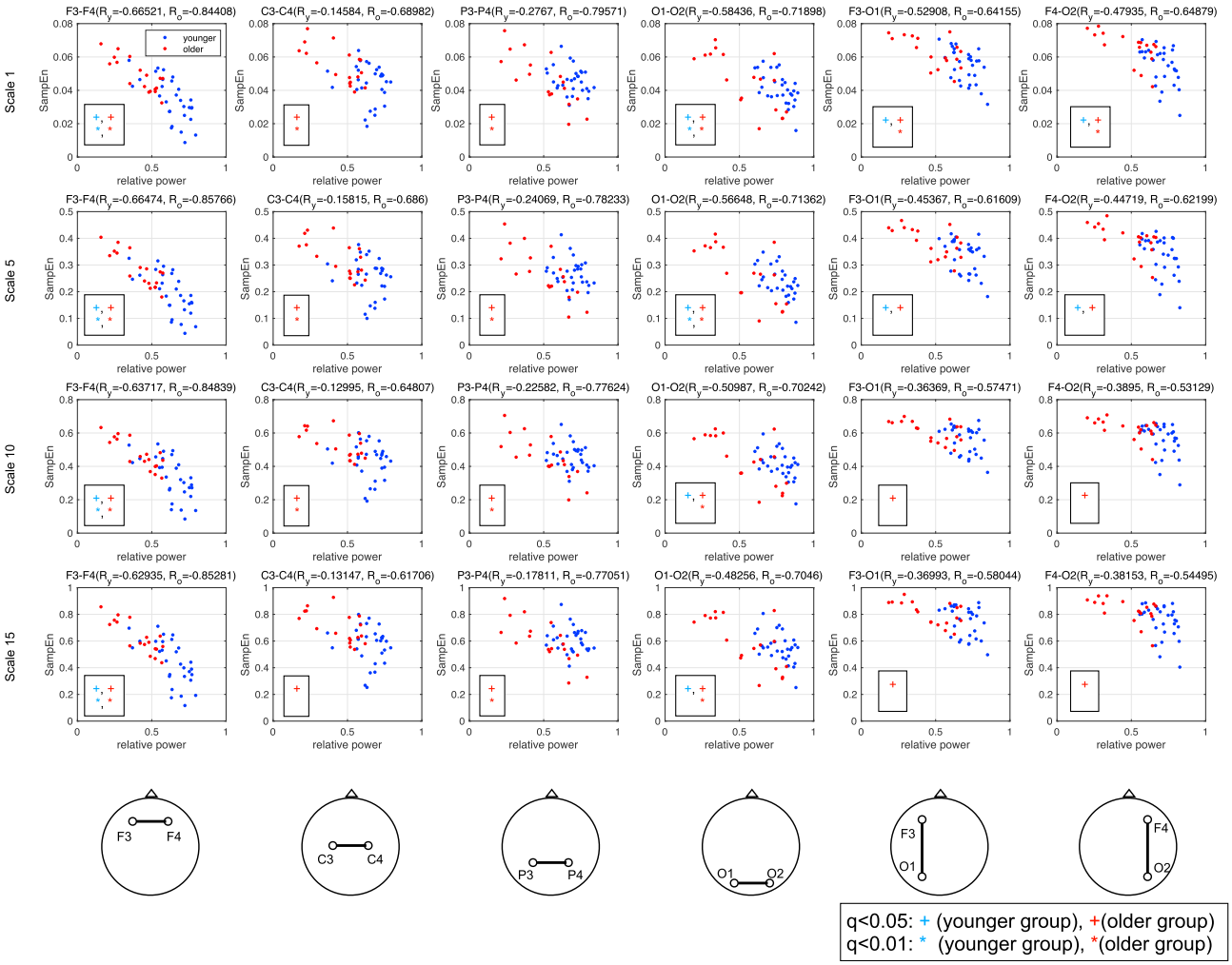

Fig. 7. Scatterplot between SampEn of DPS and relative power of alpha band. Correlation coefficients $R_{y,o}$ between them in younger and older groups, respectively. Specifically, the correlations were calculated with the averaged values for the relative alpha band powers between electrode pair corresponding with DPS.

2.5. Power spectrum analysis

Along with the PLI calculations, power spectral analysis was also performed as in conventional EEG analyses. We calculated the power spectrum density (PSD) (dB/Hz) and the relative power of the alpha band using a fast Fourier transform. A Hanning window was applied to the 60 s time-series for the calculation.

2.6. Statistical analysis

For the electrode-pair-wise group comparisons of SampEn of DPS and PLI, *t*-statistical analyses using the Benjamini—Hochberg false discovery rate (FDR) were conducted, by controlling for multiple comparisons. Specifically, *t*-scores corrected to $q < 0.05$ and $q < 0.01$ were applied for SampEn for DPS (2400 p values: 120 electrode pairs $\times$ twenty temporal scales) and PLI (120 p values: 120 electrode pairs). Similarly, for the electrode-wise group comparison of PSD, *t*-statistics adjusted using FDR correction was used. Concretely, $q < 0.05$ and $q < 0.01$ were applied for PSD (896 p values: 56 frequency points (5 − 60 Hz, width of bin is 1.0 Hz) $\times$ 16 electrodes).

For node degree of DPS and PLI, repeated measures analysis of variance (ANOVA) with group (younger vs. older) as the between-subjects factor, and nodes (16 electrodes)and time scales (twenty scales for DPS) as within-subjects factors, was performed to test for group differences. Similarly, ANOVA was applied to test for the group difference of alpha band power with group (younger vs. older) as the between-subjects factor, and node (16 electrodes) as the within-subjects factor. The Greenhouse-Geisser adjustment was applied to the degrees of freedom. To assess the significant main effect of group and the effects of interactions for electrode-wise comparisons of node degrees for DPS and PLI and of relative alpha band power, post-hoc *t*-tests were used. Here, in order to adjust for multiple comparisons, FDR correction was applied for the node degrees for DPS (320 p values: 16 electrodes $\times$ twenty temporal scales), PLI (16 p values: 16 electrodes) and the relative alpha band power (16 p values: 16 electrodes). Additionally, for correlation analysis with age, Pearson's correlations of node degrees of SampEn of DPS and PLI within each group were used.

To clarify the influence of alpha band power and instantaneous phase complexity from a single electrode to the DPS complexity, we have represented these associations using scatterplots and further calculated their Pearson's correlation coefficient values across several time scales. To control for multiple comparison in each case, FDR correction ($q < 0.01$, 0.05) was used against 2400 p values (120 electrode pairs $\times$ twenty temporal scales).

3. Results

3.1. Multiscale entropy of dynamical phase synchronization

Fig. 2 shows the results of the MSE profile of DPS and the surrogates (in which the phase components are randomized). Both the MSE profile for the original time series and their surrogates showed monotonic

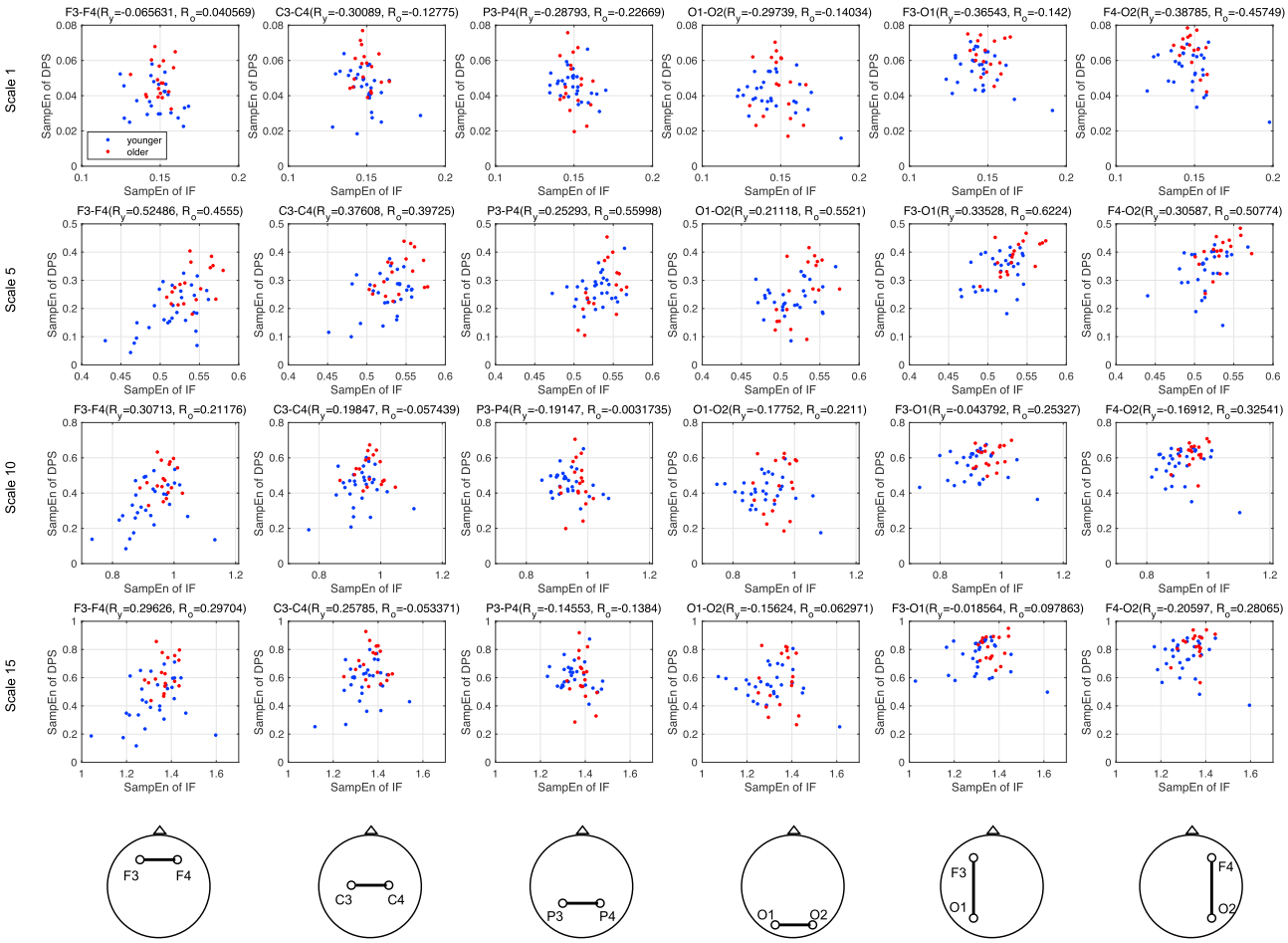

Fig. 8. Scatterplot between SampEn of DPS and SampEn of instantaneous frequency. Correlation coefficient $R_{y,o}$ between them in younger and older groups, respectively. No $R_{y,o}$ satisfies FDR criteria ($q < 0.05, 0.01$). Specifically, the correlations were calculated with the averaged values for the SampEn of instantaneous frequency between electrode pairs corresponding for DPS.

increases as a function of the time scale. However, the surrogate results demonstrated significantly higher SampEn across all time scales. In view of our simulation data of chaotic time-series (see Appendix), IAAFT significantly both reduced and enhanced SampEn alterations in a time scale-specific manner. Accordingly, we conclude that the DPS depends on nonlinear deterministic processes that are inherent in the neural network dynamics.

Fig. 3 (a) shows the SampEn of DPS for the younger group and older group and their differences at scales 1, 5, 10 and 15. *t*-tests (Fig. 3 (a), middle row) with FDR correction (Fig. 3 (a), bottom two rows) revealed significantly increased SampEn values for the older group at all scales, predominantly for electrode pairs within the frontal region and between the frontal region and other regions (i.e., central, parietal, temporal, and occipital). Table 1 summarizes the ANOVA test results for group differences in node degree of DPS complexity. We found a significant group × scale × electrode interaction. A post hoc ANOVA revealed significant group × scale, group × electrode interactions, and a main effect of group. Fig. 3 (b) shows a post hoc *t*-test for node degree of DPS controlled by FDR correction and depicts the edges (electrode pairs) that demonstrated significant group differences (Fig. 3 (b)). A significant increase in SampEn for the older group was identified, predominantly involving the frontal regions and specifically at scale 1. Regarding a possible association between age and DPS complexity, Fig. 4 shows scatter plots of the averaged node degree values of SampEn for the frontal electrodes (Fp1, Fp2, F3, F4, F7, F8, and Fz) across all ages. Correlation analysis of this averaged DPS complexity with age at scale 1 revealed no significant correlation in either younger group ($R = 0.0334$ ($p = 0.86$)) and older group ($R = 0.059$ ($p = 0.82$)).

3.2. Phase lag index

Fig. 5 (a) shows the PLI for the younger group and older group and their differences. *t*-tests with FDR correction (Fig. 5 (a), lower panels) revealed significantly reduced PLI values for the older group for several frontal electrode pairs. Table 2 summarizes the ANOVA results testing for group differences of node degree for PLI. A significant group × electrode interaction was identified without main effect of group. Fig. 5 (b) shows a post hoc *t*-test with FDR correction for node degree of PLI and depicts the edges (electrode pairs) that demonstrated significant group differences (Fig. 5 (b)). As a result, no significant group difference in node degree of PLI was identified. Correlation analysis against the node degree averaged among the frontal electrodes (Fp1, Fp2, F3, F4, F7, F8, and Fz) revealed no significant correlation between age and node degree in either the younger group ($R = 0.0035$ ($p = 0.99$)) or older group ($R = -0.025$ ($p = 0.92$)) (data not shown).

3.3. Power analysis

Fig. 6 (a) shows the dependence of average PSD for the younger and older groups. Fig. 6 (b) shows the relative power of alpha band for the younger group and older group and their statistical difference for each electrode. Visually-inspected occipitally dominant alpha power was

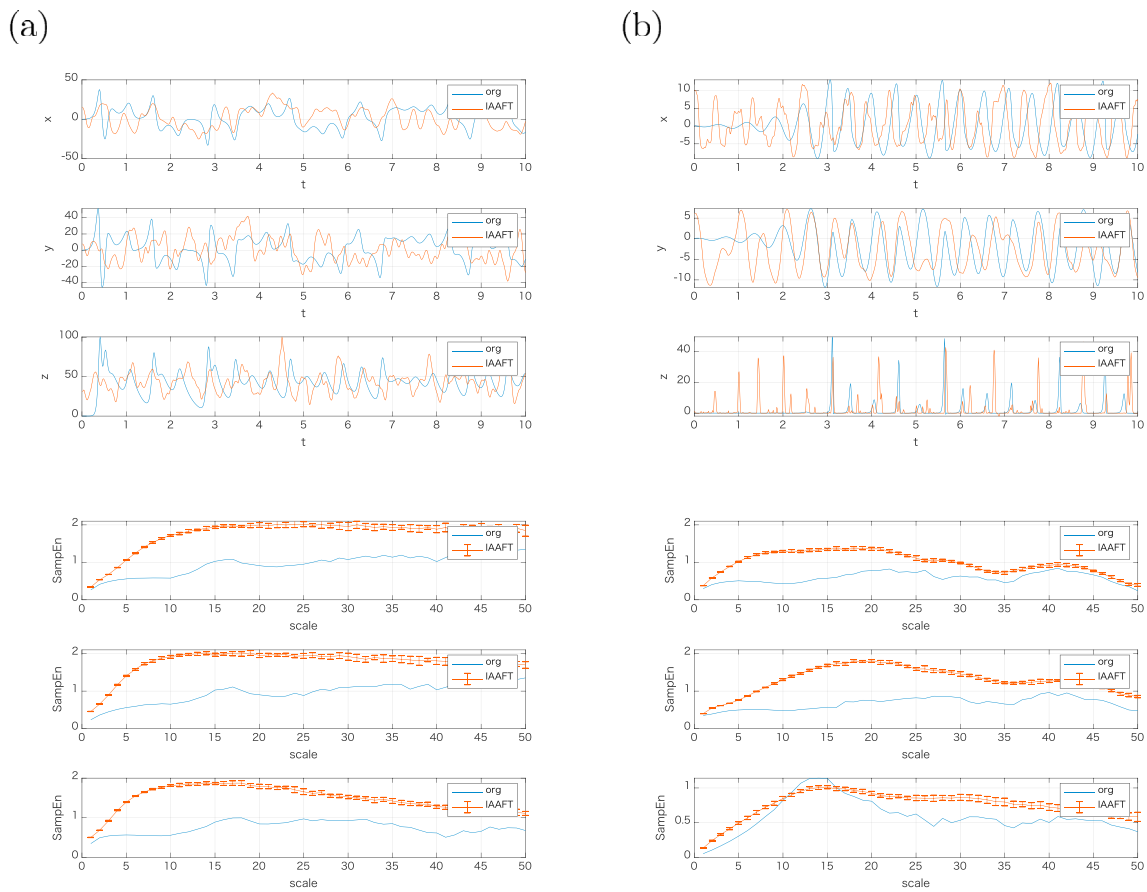

Fig. 9. Chaotic time-series and its IAAFT surrogate time-series (upper). Dependence of sample entropy (SampEn) on scale for chaotic time-series and its IAAFT surrogate time-series (lower). (a) Lorentz model. (b) Rossler model.

clearly observed in both groups. Significant reductions, predominantly in the alpha band (8 − 13 Hz) ($q < 0.05$, 0.01), were identified in the older group across all electrodes. Table 3 summarizes the post hoc ANOVA test results for group differences in the relative power of the alpha band. A significant main effect for group was identified but not for group × electrode interaction. The age-related power reduction at the alpha band is consistent with previous findings (Ishii et al., 2017).

3.4. *Correlations of DPS complexity with alpha band power and instantaneous phase complexity from single electrode*

The scatterplot of the DPS complexity and the relative alpha band power is shown in Fig. 7. Significant negative correlations ($q < 0.05$, 0.01) were observed in younger and older groups. The regional specificity of correlations differed across groups. For instance, significant correlations were identified at restricted electrode pairs in the younger group, whereas more global electrode pairs were observed in the older group (Fig. 7). Additionally, the correlation angle differed between groups (e.g., F3-F4 and F4-O2).

Fig. 8 shows the scatterplot of the DPS complexity and the instantaneous frequency complexity from a single electrode. A significant correlation ($q < 0.05$) was not observed.

4. Discussion

In this study, we examined the resting-state temporal dynamics of DPS for pairs of EEG signals using multiscale entropy, in healthy younger and healthy older groups. First, surrogate analysis revealed that the time-series of DPS involves deterministic processes. This suggests that the complexity of DPS is physiologically inherent in brain signal dynamics. Second, the results of the group comparisons indicated that compared with the younger group, the older group exhibited significantly enhanced complexity of DPS in the alpha band. Specifically, increased complexity was more prominent among electrode pairs involving frontal electrodes, particularly at short time scales. By contrast, the PLI phase synchronization approach, performed for comparison, did not identify remarkable group differences. A simple spectral analysis showed reduced alpha power in the older group, which is consistent with previous findings (Ishii et al., 2017).

Structural neuroimaging studies using the DTI method have provided extensive evidence for microstructural degradation of white matter axonal and myelin integrity with aging (Damoiseaux, 2017). In particular, age-related degradation is more prominent in the frontal white matter region than in other white matter regions (Pfefferbaum et al., 2000; Nusbaum et al., 2001; O'Sullivan et al., 2001; Grieve et al., 2007; Madden et al., 2007; Bucur et al., 2008; Sullivan et al., 2010). Several studies have demonstrated contributions of structural alterations to changes in functional connectivity. For example, white matter volume was shown to correlate with EEG functional connectivity (Smit et al., 2012). Another study demonstrated that an inherent phase gradient pattern in the resting-state EEG was absent in subjects with white matter structural damage (e.g., vascular dementia) (van Straaten et al., 2015).

An age-related reduction in interhemispheric EEG coherence has been reported across a wide frequency range, including the alpha band (Duffy et al., 1996; Kikuchi et al., 2000). Our PLI results also indicate a tendency for interhemispheric connectivity to decline within the frontal region. In contrast to these findings, our results for DPS showed more widespread age-related connectivity alterations, including changes in both intra- and inter-hemispheric connectivity, specifically involving frontal-associated brain regions, which play a critical role in various cognitive processes.

This suggests that characterizing DPS using MSE allows for capture of a new aspect of dynamic neural network communication in the aging brain. The importance of dynamic network communication analysis, which focuses on associations between temporal variability and synchronization, has been supported by Garrett et al. (2013). They proposed that a method to evaluate the covariance of temporal activity between brain regions might reflect the temporal fluctuations of dynamical networks. Interestingly, Tass et al. (1998) introduced a measure they called the ρ index, which is based on the Shannon entropy of DPS. They applied this approach to magnetoencephalography and electromyography in a Parkinsonian patient and demonstrated the importance of investigating cortico-muscular as well as cortico-cortical synchronization. We extended their ρ index concept to quantify multiple temporal-scale complexity. This extension permits characterization of temporal-scale dependent deterministic patterns in DPS.

Nevertheless, it remains unclear why the complexity of DPS was enhanced in older subjects, an outcome that seems inconsistent with the general concept that physiological complexity diminishes with aging (Goldberger et al., 2002). A reasonable explanation was presented by Voytek and Knight (2015). They constructed a theoretical framework in their review postulating that dynamic network communication reflects a balance between oscillatory coupling and local population spiking activity. A moderate strength of oscillatory coupling generates optimal synchrony of spike timing within the local neuronal populations, which is supported by many pathological and computational modeling studies (Winterer and Weinberger, 2004; Uhlhaas et al., 2006; Rolls et al., 2008; Uhlhaas and Singer, 2010; Khan et al., 2013). They argued that alterations of this oscillatory activity are associated with aging. Further, age-related cognitive decline is reportedly associated with neural noise (Cremer and Zeef, 1987). In fact, widespread alpha band power reduction observed in older subjects implies that neural noise increases with aging, which interferes with network communication. Therefore, this alpha band power reduction might result in increased DPS complexity. However, our correlation analysis revealed a correlation between DPS complexity and alpha band power in certain brain regions, with different pattern across groups. Furthermore, the enhancement of DPS complexity in the older group was prominently observed among electrode pairs involving frontal electrodes, whereas the relative alpha band reduction is observed across all electrodes relatively at occipital brain regions. These aspects may be indicative of a physiological mechanism involving alterations of DPS complexity that is different from local oscillatory alterations in the brain.

Another plausible explanation for the enhanced complexity of DPS is that chaotic synchronization (Pikovsky et al., 2003) transits to the irregular and asynchronous state in the regime of weaker connectivity. Here, chaotic synchronization is the phenomenon in which the chaotic oscillators become synchronized through stabilized mutual interactions, maintaining the chaotic/irregular behavior, under a strong enough coupling condition. From this perspective, the complexity of chaotic/irregular behavior at each oscillator does not necessarily reflect an asynchronous state. In a practical EEG used in this study, the complexity of instantaneous phase behavior from a single electrode did not influence the DPS complexity (see section 3.4). Therefore, rather than complexity from a single electrode, enhanced DPS complexity might reflect the destabilized mutual interaction among brain regions. Surrogate analysis against phase differences may also support our finding that DPS complexity increases with aging, in that significantly different profiles of the original and surrogate data might reflect the role of deterministic processes in functional connectivity.

This study has some limitations that must be considered. In this study, the distributions of age within each group is narrow, and cognitive functions were not evaluated in detail. Therefore, a longitudinal study evaluating subjects with precise cognitive function may be required to confirm our findings. In future studies, the trajectories for aging and cognitive decline must be considered by evaluating individuals of a wide age range and their cognitive function test results. Another limitation is that, in EEG, the electrical activity at each electrode might not have originated in the brain area directly underneath the electrode as neighboring EEG electrodes could have detected identical levels of brain activity. This results in "spurious" inter-regional connectivity. To solve this issue, the use of neuroimaging modalities with high spatial resolution, such as magnetoencephalography and complementary cortical source localization techniques may provide more precise spatial information. As DPS and its complexity has been estimated in this study for the first time in the field of dynamical neural networks, we initially used sensor-based conventional EEG signals. Practically, despite the low spatial resolution of EEG with spurious coherency, DPS complexity successfully detected a significant frontal-dominant age-related alternation of neural dynamics. Additionally, not only the temporal dynamics of DPS, but also approaches combining with spatial analysis may provide further insights into the spatio-temporal organization of the brain network.

5. Conclusion

In this study, we proposed a new method to capture dynamic functional connectivity using DPS and to characterize it using MSE. Although several limitations need to be considered, our findings highlight the potential usefulness of DPS in EEG studies of age-related alterations of neural dynamics. Applying this DPS analysis to neurophysiological data may provide a novel understanding of dynamical neural network processes in both healthy and pathological conditions.

Acknowledgment

This work was supported by JSPS KAKENHI Grant Number 18K18124 (SN) and JP16K10206 (TT) and Scientific Research Grant from Fukui Prefecture (TT). It was partially supported by the Center of Innovation Program from the Japan Science and Technology Agency, JST and JST CREST Grant Number JPMJCR17A4, Japan.

Appendix

The IAAFT process breaks the dynamics produced by a non-linear process. We evaluate the changes in MSE profile by the IAAFT process. As a chaotic time-series, we generated a time-series of the Lorentz model:

$$\frac{dx}{dt} = s(y - x), \tag{6}$$

$$\frac{dy}{dt} = -xz + rx - y, \tag{7}$$

$$\frac{dz}{dt} = xy - bz, \tag{8}$$

where (s, r, b) is set to $(16.0, 45.92, 4.0)$, and the time-series of Rossler model:

$$\frac{dx}{dt} = -y - z, \tag{9}$$

$$\frac{dy}{dt} = x + ay, \tag{10}$$

$$\frac{dz}{dt} = b + z(x - c), \tag{11}$$

where (a, b, c) is set to $(0.2, 0.4, 5.7)$.

Fig. 9 shows the time-series of each chaotic model and its IAAFT surrogate time-series and their MSE profile. Results of the surrogate analysis of IAAFT showed both reduced and enhanced entropy alterations depending on the time scales.

References

Aertsen, A., Gerstein, G., Habib, M., Palm, G., 1989. Dynamics of neuronal firing correlation: modulation of" effective connectivity". J. Neurophysiol. 61 (5), 900–917.

Allen, E.A., Damaraju, E., Plis, S.M., Erhardt, E.B., Eichele, T., Calhoun, V.D., 2014. Tracking whole-brain connectivity dynamics in the resting state. Cerebr. Cortex 24 (3), 663–676.

Asato, M., Terwilliger, R., Woo, J., Luna, B., 2010. White matter development in adolescence: a DTI study. Cerebr. Cortex 20 (9), 2122–2131.

Barnea-Goraly, N., Menon, V., Eckert, M., Tamm, L., Bammer, R., Karchemskiy, A., Dant, C.C., Reiss, A.L., 2005. White matter development during childhood and adolescence: a cross-sectional diffusion tensor imaging study. Cerebr. Cortex 15 (12), 1848–1854.

Bassett, D.S., Sporns, O., 2017. Network neuroscience. Nat. Neurosci. 20 (3), 353–364.

Bassett, D.S., Bullmore, E.T., Meyer-Lindenberg, A., Apud, J.A., Weinberger, D.R., Coppola, R., 2009. Cognitive fitness of cost-efficient brain functional networks. Proc. Natl. Acad. Sci. Unit. States Am. 106 (28), 11747–11752.

Bassett, D.S., Wymbs, N.F., Porter, M.A., Mucha, P.J., Carlson, J.M., Grafton, S.T., 2011. Dynamic reconfiguration of human brain networks during learning. Proc. Natl. Acad. Sci. Unit. States Am. 108 (18), 7641–7646.

Betzel, R.F., Fukushima, M., He, Y., Zuo, X.-N., Sporns, O., 2016. Dynamic fluctuations coincide with periods of high and low modularity in resting-state functional brain networks. Neuroimage 127, 287–297.

R. F. Betzel, M. A. Erickson, M. Abell, B. F. O'Donnell, W. P. Hetrick, O. Sporns, Synchronization dynamics and evidence for a repertoire of network states in resting eeg, Front. Comput. Neurosci. 6.

Blakemore, S.-J., Burnett, S., Dahl, R.E., 2010. The role of puberty in the developing adolescent brain. Hum. Brain Mapp. 31 (6), 926–933.

Braun, U., Schäfer, A., Walter, H., Erk, S., Romanczuk-Seiferth, N., Haddad, L., Schweiger, J.I., Grimm, O., Heinz, A., Tost, H., et al., 2015. Dynamic reconfiguration of frontal brain networks during executive cognition in humans. Proc. Natl. Acad. Sci. Unit. States Am. 112 (37), 11678–11683.

Bucur, B., Madden, D.J., Spaniol, J., Provenzale, J.M., Cabeza, R., White, L.E., Huettel, S.A., 2008. Age-related slowing of memory retrieval: contributions of perceptual speed and cerebral white matter integrity. Neurobiol. Aging 29 (7), 1070–1079.

Bullmore, E., Sporns, O., 2009. Complex brain networks: graph theoretical analysis of structural and functional systems. Nat. Rev. Neurosci. 10 (3), 186–198.

Buzsáki, G., Draguhn, A., 2004. Neuronal oscillations in cortical networks. Science 304 (5679), 1926–1929.

Calhoun, V.D., Miller, R., Pearlson, G., Adalı, T., 2014. The chronnectome: time-varying connectivity networks as the next frontier in fMRI data discovery. Neuron 84 (2), 262–274.

Chen, Y., Wang, W., Zhao, X., Sha, M., Liu, Y., Zhang, X., Ma, J., Ni, H., Ming, D., 2017. Age-related decline in the variation of dynamic functional connectivity: a resting state analysis. Front. Aging Neurosci. 9, 203.

Chen, Y., Zhao, X., Zhang, X., Liu, Y., Zhou, P., Ni, H., Ma, J., Ming, D., 2018. Age-related early/late variations of functional connectivity across the human lifespan. Neuroradiology 60 (4), 403–412.

Cohen, M.X., 2014. Fluctuations in oscillation frequency control spike timing and coordinate neural networks. J. Neurosci. 34 (27), 8988–8998.

Costa, M., Goldberger, A.L., Peng, C.-K., 2002. Multiscale entropy analysis of complex physiologic time series. Phys. Rev. Lett. 89 (6), 068102.

Cremer, R., Zeef, E.J., 1987. What kind of noise increases with age? J. Gerontol. 42 (5), 515–518.

Damoiseaux, J.S., 2017. Effects of aging on functional and structural brain connectivity. Neuroimage 160, 32–40.

Davison, E.N., Schlesinger, K.J., Bassett, D.S., Lynall, M.-E., Miller, M.B., Grafton, S.T., Carlson, J.M., 2015. Brain network adaptability across task states. PLoS Comput. Biol. 11 (1), e1004029.

Duffy, F.H., Mcanulty, G.B., Albert, M.S., 1996. Effects of age upon interhemispheric eeg coherence in normal adults. Neurobiol. Aging 17 (4), 587–599.

Eguiluz, V.M., Chialvo, D.R., Cecchi, G.A., Baliki, M., Apkarian, A.V., 2005. Scale-free brain functional networks. Phys. Rev. Lett. 94 (1), 018102.

Engels, M.M., Stam, C.J., van der Flier, W.M., Scheltens, P., de Waal, H., van Straaten, E.C., 2015. Declining functional connectivity and changing hub locations in Alzheimer's disease: an EEG study. BMC Neurol. 15 (1), 145.

Fries, P., 2005. A mechanism for cognitive dynamics: neuronal communication through neuronal coherence. Trends Cognit. Sci. 9 (10), 474–480.

Friston, K., Frith, C., Liddle, P., Frackowiak, R., 1993. Functional connectivity: the principal-component analysis of large (pet) data sets. J. Cerebr. Blood Flow Metabol. 13 (1), 5–14.

Garrett, D.D., Samanez-Larkin, G.R., MacDonald, S.W., Lindenberger, U., McIntosh, A.R., Grady, C.L., 2013. Moment-to-moment brain signal variability: a next frontier in human brain mapping? Neurosci. Biobehav. Rev. 37 (4), 610–624.

Glasser, M.F., Smith, S.M., Marcus, D.S., Andersson, J.L., Auerbach, E.J., Behrens, T.E., Coalson, T.S., Harms, M.P., Jenkinson, M., Moeller, S., et al., 2016. The human connectome project's neuroimaging approach. Nat. Neurosci. 19 (9), 1175–1187.

Glasser, M.F., Coalson, T.S., Robinson, E.C., Hacker, C.D., Harwell, J., Yacoub, E., Ugurbil, K., Andersson, J., Beckmann, C.F., Jenkinson, M., et al., 2016. A multi-modal parcellation of human cerebral cortex. Nature 536 (7615), 171–178.

Goldberger, A.L., Peng, C.-K., Lipsitz, L.A., 2002. What is physiologic complexity and how does it change with aging and disease? Neurobiol. Aging 23 (1), 23–26.

Grieve, S., Williams, L., Paul, R., Clark, C., Gordon, E., 2007. Cognitive aging, executive function, and fractional anisotropy: a diffusion tensor MR imaging study. Am. J. Neuroradiol. 28 (2), 226–235.

Hagmann, P., Kurant, M., Gigandet, X., Thiran, P., Wedeen, V.J., Meuli, R., Thiran, J.-P., 2007. Mapping human whole-brain structural networks with diffusion mri. PLoS One 2 (7), e597.

Hutchison, R.M., Womelsdorf, T., Allen, E.A., Bandettini, P.A., Calhoun, V.D., Corbetta, M., Della Penna, S., Duyn, J.H., Glover, G.H., Gonzalez-Castillo, J., et al., 2013. Dynamic functional connectivity: promise, issues, and interpretations. Neuroimage 80, 360–378.

Ishii, R., Canuet, L., Aoki, Y., Hata, M., Iwase, M., Ikeda, S., Nishida, K., Ikeda, M., 2017. Healthy and pathological brain aging: from the perspective of oscillations, functional connectivity, and signal complexity. Neuropsychobiology 75 (4), 151–161.

Khan, S., Gramfort, A., Shetty, N.R., Kitzbichler, M.G., Ganesan, S., Moran, J.M., Lee, S.M., Gabrieli, J.D., Tager-Flusberg, H.B., Joseph, R.M., et al., 2013. Local and long-range functional connectivity is reduced in concert in autism spectrum disorders. Proc. Natl. Acad. Sci. Unit. States Am. 110 (8), 3107–3112.

Kikuchi, M., Wada, Y., Koshino, Y., Nanbu, Y., Hashimoto, T., 2000. Effect of normal aging upon interhemispheric eeg coherence: analysis during rest and photic stimulation. Clin. Electroencephalogr. 31 (4), 170–174.

Koutsoukos, E., Maillis, A., Papageorgiou, C., Gatzonis, S., Stefanis, C., Angelopoulos, E., 2015. The persistent and broadly distributed EEG synchronization might inhibit the normal processing capability of the human brain. Neurosci. Lett. 609, 137–141.

Kubicki, M., Park, H., Westin, C.-F., Nestor, P.G., Mulkern, R.V., Maier, S.E., Niznikiewicz, M., Connor, E., Levitt, J.J., Frumin, M., et al., 2005. DTI and MTR abnormalities in schizophrenia: analysis of white matter integrity. Neuroimage 26 (4), 1109–1118.

Logothetis, N.K., 2008. What we can do and what we cannot do with fMRI. Nature 453 (7197), 869.

Madden, D.J., Spaniol, J., Whiting, W.L., Bucur, B., Provenzale, J.M., Cabeza, R., White, L.E., Huettel, S.A., 2007. Adult age differences in the functional neuroanatomy of visual attention: a combined fMRI and DTI study. Neurobiol. Aging 28 (3), 459–476.

Nolte, G., Holroyd, T., Carver, F., Coppola, R., Hallett, M., 2004. Localizing brain interactions from rhythmic eeg/meg data. In: Engineering in Medicine and Biology Society, 2004. IEMBS'04. 26th Annual International Conference of the IEEE, vol. 1. IEEE, pp. 998–1001.

Nunez, P.L., Srinivasan, R., Westdorp, A.F., Wijesinghe, R.S., Tucker, D.M., Silberstein, R.B., Cadusch, P.J., 1997. EEG coherency: I: statistics, reference electrode, volume conduction, laplacians, cortical imaging, and interpretation at multiple scales. Electroencephalogr. Clin. Neurophysiol. 103 (5), 499–515.

Nusbaum, A.O., Tang, C.Y., Buchsbaum, M.S., Wei, T.C., Atlas, S.W., 2001. Regional and global changes in cerebral diffusion with normal aging. Am. J. Neuroradiol. 22 (1), 136–142.

O'Sullivan, M., Jones, D.K., Summers, P., Morris, R., Williams, S., Markus, H., 2001. Evidence for cortical "disconnection" as a mechanism of age-related cognitive decline. Neurology 57 (4), 632–638.
Pendl, S.L., Salzwedel, A.P., Goldman, B.D., Barrett, L.F., Lin, W., Gilmore, J.H., Gao, W., 2017. Emergence of a hierarchical brain during infancy reflected by stepwise functional connectivity. Hum. Brain Mapp. 38 (5), 2666–2682.
Pfefferbaum, A., Sullivan, E.V., Hedehus, M., Lim, K.O., Adalsteinsson, E., Moseley, M., 2000. Age-related decline in brain white matter anisotropy measured with spatially corrected echo-planar diffusion tensor imaging. Magn. Reson. Med. 44 (2), 259–268.
Pikovsky, A., Rosenblum, M., Kurths, J., 2003. Synchronization: a Universal Concept in Nonlinear Sciences, vol. 12. Cambridge university press.
Rolls, E.T., Loh, M., Deco, G., Winterer, G., 2008. Computational models of schizophrenia and dopamine modulation in the prefrontal cortex. Nat. Rev. Neurosci. 9 (9), 696.
Samartzis, L., Dima, D., Fusar-Poli, P., Kyriakopoulos, M., 2014. White matter alterations in early stages of schizophrenia: a systematic review of diffusion tensor imaging studies. J. Neuroimaging 24 (2), 101–110.
Sameni, R., Seraj, E., 2017. A robust statistical framework for instantaneous electroencephalogram phase and frequency estimation and analysis. Physiol. Meas. 38 (12), 2141.
Schmahmann, J.D., Pandya, D.N., Wang, R., Dai, G., D'arceuil, H.E., de Crespigny, A.J., Wedeen, V.J., 2007. Association fibre pathways of the brain: parallel observations from diffusion spectrum imaging and autoradiography. Brain 130 (3), 630–653.
Schreiber, T., Schmitz, A., 1996. Improved surrogate data for nonlinearity tests. Phys. Rev. Lett. 77 (4), 635.
Smit, D.J., Boersma, M., Schnack, H.G., Micheloyannis, S., Boomsma, D.I., Pol, H.E.H., Stam, C.J., de Geus, E.J., 2012. The brain matures with stronger functional connectivity and decreased randomness of its network. PLoS One 7 (5), e36896.
Sporns, O., 2014. Contributions and challenges for network models in cognitive neuroscience. Nat. Neurosci. 17 (5), 652–660.
Stam, C.J., 2014. Modern network science of neurological disorders. Nat. Rev. Neurosci. 15 (10), 683–695.
Stam, C., Van Dijk, B., 2002. Synchronization likelihood: an unbiased measure of generalized synchronization in multivariate data sets. Phys. Nonlinear Phenom. 163 (3), 236–251.
Stam, C., Jones, B., Nolte, G., Breakspear, M., Scheltens, P., 2006. Small-world networks and functional connectivity in Alzheimer's disease. Cerebr. Cortex 17 (1), 92–99.
Stam, C.J., Nolte, G., Daffertshofer, A., 2007. Phase lag index: assessment of functional connectivity from multi channel eeg and meg with diminished bias from common sources. Hum. Brain Mapp. 28 (11), 1178–1193.
Stam, C., De Haan, W., Daffertshofer, A., Jones, B., Manshanden, I., Van Walsum, A.V.C., Montez, T., Verbunt, J., De Munck, J., Van Dijk, B., et al., 2009. Graph theoretical analysis of magnetoencephalographic functional connectivity in Alzheimer's disease. Brain 132 (1), 213–224.
Stebbins, G., Murphy, C., 2009. Diffusion tensor imaging in Alzheimer's disease and mild cognitive impairment. Behav. Neurol. 21 (1–2), 39–49.
Sullivan, E.V., Rohlfing, T., Pfefferbaum, A., 2010. Longitudinal study of callosal microstructure in the normal adult aging brain using quantitative DTI fiber tracking. Dev. Neuropsychol. 35 (3), 233–256.
Takahashi, T., Yamanishi, T., Nobukawa, S., Kasakawa, S., Yoshimura, Y., Hiraishi, H., Hasegawa, C., Ikeda, T., Hirosawa, T., Munesue, T., et al., 2017. Band-specific atypical functional connectivity pattern in childhood autism spectrum disorder. Clin. Neurophysiol. 128 (8), 1457–1465.
Takahashia, T., Goto, T., Nobukawa, S., Tanaka, Y., Kikuchi, M., Higashima, M., Wada, Y. Abnormal functional connectivity of high-frequency rhythms in drug-naïve schizophrenia, Clin. Neurophysiol. 129(1), pp. 222–231.
Tass, P., Rosenblum, M.G., Weule, J., Kurths, J., Pikovsky, A., Volkmann, J., Schnitzler, A., Freund, H.-J., 1998. Detection of n: m phase locking from noisy data: application to magnetoencephalography. Phys. Rev. Lett. 81 (15), 3291.
Q. K. Telesford, A. Ashourvan, N. F. Wymbs, S. T. Grafton, J. M. Vettel, D. S. Bassett, Cohesive Network Reconfiguration Accompanies Extended Training, Human Brain Mapping.
Tian, L., Li, Q., Wang, C., Yu, J., 2018. Changes in dynamic functional connections with aging. Neuroimage 172, 31–39.
Uhlhaas, P.J., Singer, W., 2006. Neural synchrony in brain disorders: relevance for cognitive dysfunctions and pathophysiology. Neuron 52 (1), 155–168.
Uhlhaas, P.J., Singer, W., 2010. Abnormal neural oscillations and synchrony in schizophrenia. Nat. Rev. Neurosci. 11 (2), 100.
Uhlhaas, P.J., Linden, D.E., Singer, W., Haenschel, C., Lindner, M., Maurer, K., Rodriguez, E., 2006. Dysfunctional long-range coordination of neural activity during gestalt perception in schizophrenia. J. Neurosci. 26 (31), 8168–8175.
van den Heuvel, M.P., Sporns, O., 2013. Network hubs in the human brain. Trends Cognit. Sci. 17 (12), 683–696.
van den Heuvel, M., Mandl, R., Luigjes, J., Pol, H.H., 2008. Microstructural organization of the cingulum tract and the level of default mode functional connectivity. J. Neurosci. 28 (43), 10844–10851.
van Straaten, E., Den Haan, J., De Waal, H., Van der Flier, W., Barkhof, F., Prins, N., Stam, C., 2015. Disturbed phase relations in white matter hyperintensity based vascular dementia: an eeg directed connectivity study. Clin. Neurophysiol. 126 (3), 497–504.
Varela, F., Lachaux, J.-P., Rodriguez, E., Martinerie, J., 2001. The brainweb: phase synchronization and large-scale integration. Nat. Rev. Neurosci. 2 (4), 229–239.
Voytek, B., Knight, R.T., 2015. Dynamic network communication as a unifying neural basis for cognition. development, aging, and disease, Biological psychiatry 77 (12), 1089–1097.
Winterer, G., Weinberger, D.R., 2004. Genes, dopamine and cortical signal-to-noise ratio in schizophrenia. Trends Neurosci. 27 (11), 683–690.
Zalesky, A., Fornito, A., Cocchi, L., Gollo, L.L., Breakspear, M., 2014. Time-resolved resting-state brain networks. Proc. Natl. Acad. Sci. Unit. States Am. 111 (28), 10341–10346.
Zhang, Y., Schuff, N., Jahng, G.-H., Bayne, W., Mori, S., Schad, L., Mueller, S., Du, A.-T., Kramer, J., Yaffe, K., et al., 2007. Diffusion tensor imaging of cingulum fibers in mild cognitive impairment and Alzheimer disease. Neurology 68 (1), 13–19.
Zhang, J., Cheng, W., Liu, Z., Zhang, K., Lei, X., Yao, Y., Becker, B., Liu, Y., Kendrick, K.M., Lu, G., et al., 2016. Neural, electrophysiological and anatomical basis of brain-network variability and its characteristic changes in mental disorders. Brain 139 (8), 2307–2321.